A THEORETICAL STUDY ON NLO PROPERTY OF COBALT COMPLEX BASED ON DENSITY FUNCTIONAL THEORY

Dissertation Submitted
to the University of Kerala for the Partial Fulfilment of Requirement
for the Award of the Degree of

MASTER OF SCIENCE
in PHYSICS
By

FATHIMA FAZAL (REG.NO: 63022101006)

Department of Physics

Bishop Moore College, Mavelikara

Affiliated to

UNIVERSITY OF KERALA, INDIA

Under the guidance of

Dr.LYNNETTE JOSEPH
Assistant Professor
Department of Physics
Bishop Moore College, Mavelikara

Project report 2024

A THEORETICAL STUDY ON NLO PROPERTY OF COBALT COMPLEX BASED ON DENSITY FUNCTIONAL THEORY

Post Graduate and Research Department of Physics
Bishop Moore College, Mavelikara

Dissertation submitted to the University of Kerala in partial Fulfilment for the degree of M.Sc. in Physics

Name	**:**	**FATHIMA FAZAL**
Class	**:**	**MSc Physics**
No	**:**	**44382**
Year	**:**	**2022-2024**
University Reg. No	**:**	**63022101006**
Year of Appearance	**:**	**2024**

CERTIFIED GENUINE

Signature of Lecture in charge:

Signature of Examiners: 1.

2.

Date:

CERTIFICATE

This is to certify that the dissertation entitled "**A THEORETICAL STUDY ON NLO PROPERTY OF COBALT COMPLEX BASED ON DENSITY FUNCTIONAL THEORY**" is an original and independent work done by **FATHIMA FAZAL (Reg.No: 63022101006)** in partial fulfilment for the award of the degree of **Master of science** in physics at the **Department of Physics, Bishop Moore College, Mavelikara.** It is a bonafide work carried out by him, under my guidance and supervision during the academic year 2022-2024. This dissertation partially or fully has not been submitted by any other degree or diploma of this university or other universities.

Dr. LYNNETTE JOSEPH

Assistant Professor

(Supervising Guide)

DECLARATION

I, **FATHIMA FAZAL,** hereby state that the dissertation entitled **"A THEORETICAL STUDY ON NLO PROPERTY OF COBALT COMPLEX BASED ON DENSITY FUNCTIONAL THEORY''** submitted during the academic year 2022-2024 for the award of Degree of **Master of Science in Physics** is an authentic work carried out by me under the guidance of **Dr. LYNNETTE JOSEPH**, Assistant Professor , Department of Physics, Bishop Moore College, Mavelikara, Kerala. I also declare that this work has not been submitted for any other degree.

Place: Mavelikara **FATHIMA FAZAL**

Date:

ACKNOWLEDGEMENT

I am immensely happy to present this dissertation as a part of my Master of Science Programme. At this outset, I would like to express my gratitude to various people who have helped me at different stages of this work.

In the first place, I would like to express my deepest gratitude to my guide, Dr LYNNETTE JOSEPH , Assistant Professor, Department of Physics, Bishop Moore College, Mavelikara, for his guidance and support throughout the course of this project. His insightful feedback and encouragement were instrumental in shaping this research.

I take privilege to acknowledge my indebtedness and respectful gratitude to Mrs. Jerin Susan John, Assistant Professor Department of Physics, Bishop Moore College, Mavelikara for her consistent guidance and valuable advices during the entire period of the work that helped me to bring the study into success. I would like to explicit my sincere gratitude to all the faculty members, Bishop Moore College, Mavelikara for their encouragement and support in the development of the work.

I am also profoundly thankful to Dr. D Sajan , Professor and Head of the Physics department, Bishop Moore College, Mavelikara, for providing the resources and conducive environment necessary for the successful completion of this project. The facilities and academic support offered by the institution were crucial to my research.

My heartfelt thanks to Mr Saji Chandran, Research Scholar, Department of Physics, Bishop Moore College, Mavelikara, whose collaboration and discussions greatly enriched my understanding of the subject. Their shared knowledge and camaraderie made the research process both productive and enjoyable.

Lastly, I would like to acknowledge my family and friends for their unwavering support and encouragement, which sustained me throughout this academic journey.

FATHIMA FAZAL

ABSTRACT

The metal-organic crystal Diaquabis (nitrato)-bis(1λ5-pyridine-1-olato)-cobalt was synthesized and single crystals were grown by slow evaporation technique. Density Functional Theory was used to obtain the theoretical calculations using the Gaussian program package. B3LYP/def2TZVP/LANL2DZ level of theory was used to get the geometrical optimization of the title compound, in this compound electronic analysis studies carried out by DFT. Different types of analysis done by DFT can reveal possible types of electron interactions such as inter-atomic and intra-atomic. Hirshfield surface also boosts this evidence. From this research, the hyperpolarizability of the compound is calculated with good values. These coefficients of polarizability and hyperpolarizability values indicate the title compound is suitable for the NLO mechanism and application.

CONTENTS

CHAPTER 1

INTRODUCTION

Density functional theory (DFT) is a quantum-mechanical method used to calculate the electronic structure of atoms, molecules, and solids. It is studied with the computational quantum mechanical modeling technique in physics, chemistry, and material science. DFT is the most widely used electronic structure method, computational physics, condensed [1]. The ground state, electronic structure, of many-body systems, particularly atoms, molecules, and condensed phases, is studied with the computational quantum mechanical modeling technique known as density–function theory (DFT) in the fields of physics, chemistry, and material science. The quantum mechanical investigations on the structure, vibrational spectra, and DFT calculations on the crystal Diaquabis(nitrato)-bis(1λ5-pyridin-1-olato)-cobalt are expected to be done in this project. Computational quantum chemistry, which uses many approximation methods, including Density functional theory is used in this work to obtain necessary information about the many-electron system under study.

Hirshfield analysis method is a tool for visualizing interactions in molecular crystals. Hirshfield surfaces are created by an extension of the weight function describing an atom in a molecule to describing an atom in a molecule to include the function of a molecule in a crystal. It was identified as the space occupied by a unit cell in a crystal system based on the electron distribution calculated around the spherical electron density in each atom. Infrared spectroscopy (IR) is widely used to study catalysts and molecules absorbed. The theory behind this technique is based on the interaction of electromagnetic radiation and a species that has a permanent or induced dipole moment. This technique is highly sensitive to molecular vibration and can discriminate geometrical distortions present in adsorbed molecules [2]. The vibrational spectrum is a method of measuring and displaying the vibration signals of a rotating machine as a function of frequency. It is a graph that shows the frequencies – amplitudes of a vibration signal. Vibrational spectra refer to the characteristic features of a molecule that can be identified and analyzed through Raman and

infrared spectroscopy. It allows for the identification of chemical species and the elucidation of their structure and dynamics.

Nonlinear optics, which studies the interaction of the intense light field with matter, is a relatively new field with lots of fundamental scientific and technological potential applications. Nonlinear optics is concerned with the propagation of intense beams of light through a material system. It brought many technological advances through the study of nonlinear optics in new structures such as quantum wells and optical fibers. NLO crystals play an important role in the field of photoelectronic, optical communication, optical modulators, laser spectroscopy, frequency conversion, and so on. Semi–organic crystals exhibit high NLO response, thermal stability, laser damage threshold, mechanical stability, wide optical window transmittance, and structural diversity. combinations of inorganic and organic molecules yield semi-organic crystals.

The discovery of new crystals for optical applications has been an emerging area of research, along with the increased studies on the optical properties of materials. Both organic and inorganic materials are studied extensively. Crystals with nonlinear optical response (NLO)are significant in science and modern technology because of their technological importance in the areas of optical communication, information processing, data storage, etc. Usually, organic materials show excellent NLO properties and hence the growth of new organic-based single crystals is important. The hyperpolarizability, a nonlinear optical property of a molecule, is the second-order electric susceptibility per unit volume. It provides a complete description of the electric dipole moment (μ), the dipole polarizability(α), the first dipole polarizability(β), the second dipole polarizability (γ) can be calculated. β is a quantitative measurement of the change in the charge distribution of an atom or a molecule when it interacts with an electromagnetic wave. The hyperpolarizability can be calculated using quantum chemical calculations developed in software packages.

A new interdisciplinary research approach that brings people together, computational material science or computational physics. Elements of different fields of study such as physics, chemistry, mathematics, biology and engineering, and even medicine. Multiscale and multidisciplinary stimulations can also be performed in realistic situations using this method. This allows us to determine the structure and properties of the molecule. Arithmetical results usually complement the information obtained from experimental results.

CHAPTER 2

LITERATURE REVIEW

Niazi M, Klein A, et al. in their work studied the structural and spectral properties of the monomolecular entities of these compounds using DFT and TD-DFT. All calculations were performed using the Gaussian 09 programs. Geometry optimizations and calculations of all complexes were carried out in DMSO as solvent using DFT. They computed the molecular geometries, IR spectra, and energy together with UV-Vis spectra using M06-2X functional and LANL2DZ ECP and def2TZVP as basis sets. Recently reported DFT and TD-DFT calculations on the molecular and electronic structures of planar d^8 configured Ni^{II} ,Pd^{ii} , and Pt^{II} complexes have shown that the reliability of calculated data with experimental data is very dependent on functionals and basis sets.

B. Narayana Moolya,A . Jayarama studied Fourier transform infrared spectral technique, second harmonic generation, X-ray diffraction, and nonlinear optics on the single crystal of γ-glycine, which was grown by solvent evaporation from a mixture of aqueous solutions of glycine and ammonium nitrate at ambient temperature. FTIR was employed to characterize the crystal. Nonlinear optical characteristics of GG were studied using Q switched Nd: YAG laser and the SHG conversion efficiency of GG is 1.5 times that of potassium dihydrogen phosphate. They reported that the X-ray diffraction and Fourier transform infrared spectra showed the presence of strong hydrogen bonds which create and stabilize the crystal structure in GG. NLO contribution results from the presence of the hydrogen bond and the vibrational part due to very intense infrared bands of the hydrogen bond vibrations [17].

Tongpeng Zhao et al. synthesized a new promising NLO material 1-(-4-methoxyphenyl)-3-(4-N, N dimethyl aminophenyl)-2-propen-1-one(damo). Its high–quality crystal was grown by slow evaporation technique. The single crystal XRD revealed the structure of the crystal and the FTIR and ^1H NMR spectroscopy confirmed all the functional groups of the crystal. The experimental

data on the thermal, optical, and dielectronic properties of the crystal were analyzed systematically. The SHG efficiency of DAMO was obtained as 42.71 times that of KDP crystal and was confirmed by the Kurtz-Perry powder technique [18].

Mohamed Boukabene et al. in their paper report the structural, optical, and nonlinear properties, of UV-Vis absorption spectra of four cyclomelated [Ir(dFNppy)2(PPh3)L] using DFT and TD-DFT methods. Compared structural parameters of the complexes are similar to experimental data. Experimental absorption bands were assigned based on natural transition orbitals and the intense band observed in the UV region corresponds mainly to intra-ligand charge transfer. The optical properties, the static first hyperpolarizabilities electric-field induced second harmonic generation, the hyper-Rayleigh scattering first hyperpolarizability, and the depolarization ratio of these complexes are calculated by DFT [20].

Samrah Kamal in his work, two water-stable Cd(II) metal-organic clusters using a slow evaporation method are designed and synthesized. The synthesized complexes such as $[Cd_2(pda)_2(H_2O)_6]$. $(H_2Pda)_2$ and $[Cd_4(HPda)_4(\mu_2\text{-}OH)_{2)}(Cl)_2(H_2O)_6].2H_2O$ .FTIR spectra were recorded on the spectrophotometer. The two complexes were characterized by various spectroscopic studies and with the help of a single crystal technique the structures were elucidated. The metal-organic clusters exhibit various non-covalent interactions which were further verified by Hirshfield surface analysis. The DFT calculations were also performed on both the complexes with the electronic and spectral aspects of complexes [21].

Poornima S. Liyanage reported in their work the design of novel organometallic systems that show enhanced NLO activity. First static hyperpolarizability (β) of nitrogen-bound low valent (M^0) group six metal carbonyls representing the class of chromophores displaying weak coupling between donor and acceptor is calculated utilizing high accuracy Density Functional Theory (DFT) using GAUSSIAN98W. The geometry optimizations of chromium and tungsten carbonyls were performed using the DFT method at the B3LYP/LanL2DZ level of theory using GAUSSIAN98W. The molecular HOMO and LUMO were examined [22].

Paulo J. Mendes studied the static first hyperpolarizability (β) for a series of both substituted thiophene- acetylide ligands and the corresponding η^5 – monocyclopentadienyliron (II) complexes were determined by density functional theory (DFT) calculations. The effect on the hyperpolarizabilities by various donor and acceptor substituents in the thiophene–acetylide ligands

was studied. For understanding electronic factors responsible for the second-order nonlinear optical properties of η^5 –monocyclopentadienyliron (II) complexes with substituted thiophene-acetylide ligands, used density functional theory calculations as well as TD-DFT [23].

CHAPTER 3

THEORETICAL BACKGROUND

3.1 DENSITY FUNCTIONAL THEORY

Density functional theory (DFT) is a theory of electronic structure, based on the electron density distribution n(r), instead of the many-electron wave function Ψ(r1,r2,…)[1]. It is a quantum-mechanical method used to calculate the electronic structure of atoms, molecules, and solids. It is studied with computational quantum mechanical modeling techniques in the fields of physics, chemistry, and material science. DFT is the most widely used electronic structure method, computational physics, and condensed matter physics [2]. In an atom that consists of a nucleus and electrons where atomic nuclei are heavier than individual electrons and electrons respond much more rapidly to changes in their surroundings than nuclei. The time-independent Schrodinger equation is HΨ=EΨ where H is the Hamiltonian operator and Ψ is the eigenstates, having eigenvalue E_n, a real number that satisfies the eigenvalue equation. In other words, the Schrodinger is,

$$[\frac{h^2}{2m}\sum_{i=1}^{N}\nabla^2+\sum_{i=1}^{N}\sum_{j<i}u(r,r)]\Psi=E\Psi \quad (1)$$

Where m is the mass of the electron

The other terms are kinetic energy of each electron, the interaction energy between each electron and atomic nuclei, and the interaction energy between different electrons.

The Hamiltonian in which Ψ is the electronic wave function contains the spatial coordinates of N electrons and E is the ground state energy of the electrons. As the E is independent of time, so it is a time-independent Schrodinger equation. It is possible to approximate Ψ as a product of individual electron wave function, $\Psi_1(r_1)\ \Psi_2(r_2)\ \ldots\ldots\Psi_N\ (r)$. This expression for the wave function is known as a Hartree product. But the team in the Hamiltonian defining electron-electron interaction is the most critical one in which $\Psi_i(r\ )$, cannot be found out without simultaneously considering the individual; electron wave functions associated with all other electrons. That is, the Schrodinger

equation is a many-body problem. In the Schrodinger problem, we can determine the probability that the N electrons are at a particular set of coordinates r_1,….r_N.[3]

2.1.1 FUNCTIONAL

The function is the electron density, which is a function of space and time. The electron density directly deals with many body wavefunctions having 3N variables. By Hohenberg and Kohn is the ground state energy from Schrodinger's equation is a unique function of the electron density. There exists a one-to-one mapping between the ground state wave function and the ground state electron density. A function takes a value of variables i.e. F[f]. The ground state energy E can be expressed as E[n(r)], where n (r) is the electron density. The ground state electron density determines all properties, including the energy and wavefunction of the ground state. This is the first Hohenberg – Kohn theorem in which the function of electron density exists that can be used to solve the Schrodinger equation but says nothing about what a function is.

The second Hohenberg-Kohn theorem is the electron density that minimizes the energy of the overall function is the true electron density corresponding to all solutions of the Schrodinger equation. The electron density, n (r). The electron function is

$$\boldsymbol{E}[\{\boldsymbol{\varphi_i}\}] = \boldsymbol{E_{known}}[\{\boldsymbol{\varphi_i}\}] + \boldsymbol{E_{XC}}[\{\boldsymbol{\varphi_i}\}] \quad (2)$$

The known terms include:

$$E_{known}[\{\Psi_I\}] = h\hat{}2/m\sum_i \int \Psi^* \Delta^2 \Psi \, d^3r + \int v(r)n(r)d^3 r + e^2/2 \iint n(r)n(r')\frac{d^3r d^3r'}{r\,r'} + E_{ion} \quad (3)$$

The terms are electron kinetic energies, the culombic interactions between pairs of electrons and nuclei, the coulombic interactions of pairs of electrons, and the culombic interaction between pairs of nuclei. The complete energy functional $E_{XC}[\{\Psi_i\}]$, is the exchange correlation functional.

For finding the right electron density can be expressed as solving a set of equations in which each equation only involves a single electron. The Kohn-sham equation has the form

$$\left[\frac{\boldsymbol{h^2}}{\boldsymbol{2m}}\boldsymbol{\nabla^2} + \boldsymbol{V(r)} + \boldsymbol{v_H(r)} + \boldsymbol{Vxc(r)}\right]\boldsymbol{\varphi(r)} = \in \boldsymbol{\varphi(r)} \quad (4)$$

There is no summation because the solution of the Kohn sham equations is single electron wave functions that depend only on three spatial variables $\Psi_i(r)$.

Where,

$$\boldsymbol{v_H(r) = e^2 \int \frac{n(r')}{|r\, r'|} d^3 r'} \quad (5)$$

This potential describes the coulombic repulsion between the electron and the total electron density. The Hartree potential includes a so-called self-interaction contribution.

V_{XC} can be defined as a functional derivative of exchange-correlation energy [4].

$$\boldsymbol{Vxc\ (r) = \frac{\delta Exc(r)}{\delta n(r)}} \quad (6)$$

2.1.2. BASIS SET

Basis sets are used to guess the electronic wave functions for Hartree Fock, which deal with the wave function of every electron. Basis functions can be considered as representing the atomic orbitals of the atoms and are introduced in quantum chemical calculations because the equations defining the molecular orbitals are otherwise very difficult to solve. In principle, a user would employ the largest basis set available to model molecular orbitals as accurately as possible. In practice, the computational cost grows rapidly with the size of the basis set so a compromise must be sought between accuracy and cost [5]. Basis sets can be constructed from slater, Gaussian, plane wave, and delta functions.

A finite set of basic functions are used to perform calculations. When the finite basis is expanded towards a complete set of functions, calculations employing such a basis set are said to approach the complete basis set (CBS) limit. Such basic functions are centered on the atoms and are referred to as Atomic Orbitals (AO). Each electron can be viewed to be limited to a particular region of space due to the basis set. Smaller basis sets impose more constraints on the electrons, while larger ones cause fewer restrictions and approximate each orbital more accurately. However, larger basis sets require more computational resources [6].

Two types of basis set:

1. Slater Type Orbitals (STOs)

2. Gaussian Type Orbitals (GTOs)

In Slater type orbital basis code for density functional theory calculations to include "exact exchange" so that Hartree Fock and Hybrid DFT is performed. As the most variational method calculations, a larger basis set improves the accuracy of the calculations by providing more variable parameters to produce a better approximate wave function. Historically effective nuclear charge of the nucleus was estimated by Slater's rule. STOs describe the radial part of the function as:

$$\boldsymbol{R(r) = Nr^{n-1}e^{-\xi r}} \tag{7}$$

Where n is a natural number that plays the role of principal quantum number, n=1,2,3….., N is a normalizing constant, r is the distance of the electron from the atomic nucleus and ξ is a constant related to the effective charge of the nucleus, the nuclear charge being partially shielded by electrons.

The most efficient and fastest codes use an auxiliary basis set to fit the density so that only three center integrals need to be evaluated. The codes DGAUSS and TURBOMOL use Gaussian basis sets, whereas the long-established ADF code uses Slater basis sets [5]. The choice of basis set in quantum chemical calculations can have a huge impact on the quality of the results, especially for correlated *ab initio* methods [6]. There is a list of Gaussian basis sets that are optimized to perform accurate molecular calculations based on DFT. It targets a wide range of chemical environments, including the gas phase, interfaces, and the condensed phase. For a given accuracy in the total energy, fewer basis functions are needed than in the usual split valence scheme, leading to a speedup for systems where the computational cost is dominated by diagonalization [7].

A Gaussian basis function has the form,

$$\boldsymbol{G_{nlm}(r,\theta,\varphi) = N_n r^{n-1} e^{-ar2} Y_1^m(\theta,\varphi)} \tag{8}$$

The use of a minimum basis set puts a restriction on the variation that can be made on the electronic charge, to describe molecules and chemical bonds, from the free electronic charge distribution in the free atom.

2.2 GEOMETRY OPTIMIZATION

Geometry optimization is a very important step in computational chemistry studies that are focused on the structure and/or reactivity of molecules. The structure of a molecule can be pointed out but providing the atomic locations in the molecule. A molecule has a specific energy for a given structure and electronic state. The variation of the energy of the molecule in a particular state as a function of the structure of the molecule is given by a potential energy surface. The potential energy surface (PES) which is a central concept in computational chemistry, and has very much importance in the analysis of molecular geometry and chemical reaction dynamics. It is because, they help us to visualize and understand the relationship between the potential energy and the molecular geometry, and to understand how computational chemistry programs locate and characterize structures of interest. The minimum and the saddle points are the important points of interest and are called stationary points. The minimum and the saddle points are the important points of interest and are called stationary points. The first derivative of the energy vanishes at these points. Since the negative of the gradient is the vector of forces on the atoms in the molecule, the forces are also zero at these points. Thus, stationary points are points on the potential energy surface where the forces are zero.

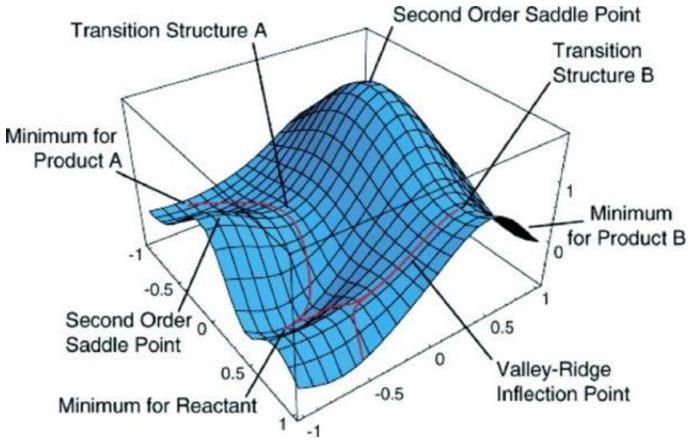

Fig.1 Features of potential energy surface

Regarding computational chemistry, Geometry optimization (also called energy optimization or energy minimization) is the process of finding an arrangement of a collection of atoms in space

such that the net inter-atomic force on an individual atom is close to zero and the position on the potential energy surface (PES) is a stationary point. A single molecule, an ion, a condensed phase, a transition state, or even a collection of any of these may be regarded as a collection of atoms. Usually, the potential energy surface may have more than one Local Minimum and one Global Minimum (lowest energy points in PES).

The geometry optimization process involves the calculation of the wave function and the energy at a starting geometry and then proceeding to find a new geometry of lower energy. The iteration goes on until the lowest energy geometry is obtained. The first derivative (or gradient) to atomic positions is evaluated in the force on each atom. Then for a rapid convergence to the lowest energy geometry, refined algorithms are used to select a new geometry, at each step. The result converges to the final minimum energy geometry for which the force on each atom is zero, at one point. It should be noted that this procedure does not guarantee the lowest energy geometry as a result (global minimum in the PES diagram).

Frequency calculation

The nuclei in molecules are in continuous motion in the practical case. At equilibrium states, these vibrations are regular and hence, predictable. Then the molecule can be identified because of its characteristic spectra. The vibrational spectra of the molecules in their ground and excited states can be computed by the chemical computation software. The program can predict the frequencies and intensities of spectral lines, and also it can describe the normal mode vibrations executed by the system. The program also predicts the direction and magnitude of the nuclear displacement occurring in the system on absorbing a quantum of energy. The frequency calculations must be done on optimized structures since the frequency calculations are valid only at stationary points on the PES.

2.3. HIRSHFELD ANALYSIS

Hirshfield analysis is a powerful technique to visualize intermolecular interactions in the crystalline state and to explore the X-ray information. HS is used to determine the space location of contact between different fragments of the molecule. Moreover, associated 2D fingerprint plots (FP) present a rapid quantitative summary. HS maps illustrate the interatomic contacts based on the electron distribution calculated as the sum of spherical atom electron densities. The normalized contact distance, d_{norm} , based on d_e and d_i lengths (from the HS to the nearest atom outside – external and inside – internal the surface, respectively)and the Van der Waals radii of the atom (r^{vdw}), given by the equation, enables identification of the regions of particular importance to intermolecular interactions [32].

$$\boldsymbol{d_{norm}} = \frac{\boldsymbol{d_i - r_i^{vdw}}}{\boldsymbol{r_i^{vdw}}} + \frac{\boldsymbol{d_e - r_e^{vdw}}}{\boldsymbol{r_e^{vdw}}} \quad (9)$$

Hirshfield surfaces were named after F. L Hirshfield, whose "stockholder partitioning" scheme for defining atoms in molecules suggested to us an extension to defining a molecule in a crystal. Distances from the Hirshfield surface to the nearest nucleus inside the surface and outside the surface were the first functions of distance explored for mapping on the surfaces. The fingerprint plot was invented to overcome the difficulty of representing in a 2D format two different but potentially useful distance measures, each mapped on 3D-molecular surfaces [33]. Hirshfield Analysis is done using Crystal Explorer 21.5 TONTO software.

2.4. INFRARED SPECTROSCOPY

Infrared spectroscopy deals with the infrared region of the electromagnetic spectrum i.e. light having a longer wavelength and a lower frequency than visible light. Infrared spectroscopy generally refers to the analysis of the interaction of a molecule with infrared light. The IR spectroscopy can be analyzed in three ways: by measuring reflection, emission, and absorption. The IR spectroscopy theory utilizes the concept that molecules tend to absorb specific frequencies of light that are characteristic of the corresponding structure of the molecules. The energies are

reliant on the shape of the molecular surfaces, the associated vibronic coupling, and the mass corresponding to the atoms. A molecule composed of n-atoms has 3n degrees of freedom, six of which are translations and rotations of the molecule itself. This leaves 3n-6 degrees of vibrational freedom (3n-5, if the molecule is linear). Vibrational modes are such as stretching, bending, scissoring, rocking, and twisting.

Vibrational spectroscopy involves the interaction of infrared radiation with inorganic chemicals and covers a range of techniques, mostly based on absorption spectroscopy. It can be used to identify and study inorganic chemicals. IR spectroscopy is one of the most common and widely used spectroscopic techniques. Absorbing groups in the infrared region absorb within a certain wavelength region. The absorption peaks within this region are usually sharper when compared with absorption peaks from the ultraviolet and visible regions. A basic infrared spectrum is a graph of infrared light absorbance (or transmittance) on the vertical axis vs frequency or wavelength on the horizontal axis. Typical units of frequency used in an infrared spectrum are reciprocal centimeters(cm^{-1}). Fourier transform infrared, more commonly known as FT-IR, is the preferred method for infrared spectroscopy. Developed to overcome the slow scanning limitations encountered with dispersive instruments, with FT-IR the infrared radiation is passed through a sample. The measured signal is referred to as an interferogram.

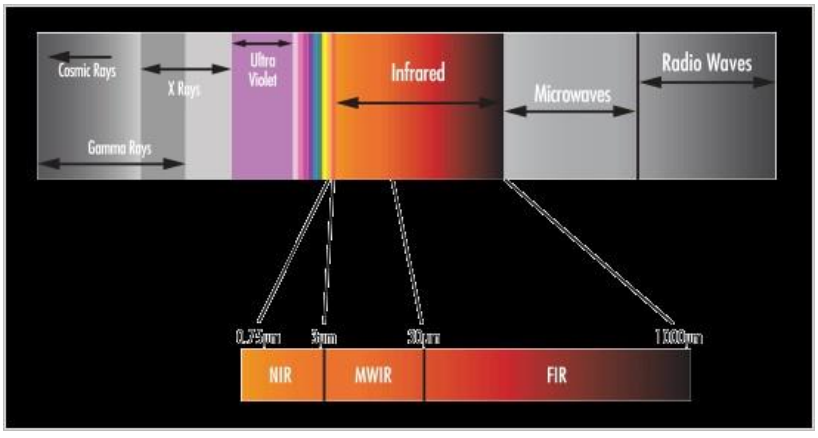

Fig 2: Electromagnetic spectrum (sourse [2])

When IR radiation is passed through the IR active compounds, they will get excited and show specific vibrational rotational spectra, which are characteristic to the functional group of compounds. The frequency and wavelength of absorption relative to the mass of the atom, force constant of bonds, and geometry of atoms. The band position in IR spectra is represented as a wavenumber i.e.$\bar{\nu}$.

$$\bar{\nu} = {}^{1}/_{\lambda}\textbf{(Wavelength)} \tag{10}$$

Transmittance (T) represents the bond intensities.

$$\boldsymbol{T = I/I_0} \tag{11}$$

Where, I=intensity of transmitted light

I_0=intensity of incident light

2.5. NATURAL BOND ORBITAL ANALYSIS

Natural bond orbital (NBO) analysis is one of the methods for translating computational solutions of Schrodinger's wave equation into chemical bonding concepts. NBO descriptors in Hammett-type quantitative structure-activity relationships; nature of conventional and anti-electrostatic hydrogen bonding interactions high -order multiple bonding in transition metal species etc.[17].NBO method to complement chemical structure and reactivity. It underlies the methods and implementation in a computer program that provides such analysis of quantum chemical calculations. NBO-based description of an Abintio or density functional theoretic calculation differs from other methods in its "natural" focus on eigen properties of the first order density operator ($\Gamma^{(1)}$) , rather than the energetic properties featured in energy decomposition analysis.NBO analysis involves converting nonorthogonal atomic orbitals (AO) to natural atomic orbitals (NAO), hybrid orbitals (NHO), and bonded orbitals (NBO) by sequentially converting the complete and orthogonal sets. It is based on the optical conversion of a given wave function into a local form corresponding to the single–center ("lone pair") and double-center ("bond") elements of the Lewis structure diagram. The NBO localization protocol divides the NBO into core, bond-

forming, anti-bond-forming, and "Rydberg" (residual)orbitals. The core and bond-forming orbitals describe strictly the localized Lewis structure of the molecule. The sequence passes through various local bases set in the order [18].

$$\boldsymbol{AO \rightarrow NAO \rightarrow NHOs \rightarrow NBOs \rightarrow NLMOs \rightarrow CMOs} \quad (12)$$

The natural bond orbitals (NBOs)are one-centered or two-centered localized orbitals that give a Lewis-type description of the chemical bond. Each one-centered(1c)lone pair or two-center(2c) bond pair of the Lewis structure is related to a 'Lewis' (L type)member of the complete orthonormal set of NBOs, where the completion of the span of the basis and the description of the residual resonance delocalization effects are done by the remaining 'non-Lewis' (L type)member of the complete orthonormal set of NBOs, where the completion of the span of the basis and the description of the residual resonance delocalization effects are done by the remaining 'non-Lewis'(NL) type.

$$\boldsymbol{\Omega_{AB} = C_A h_A + C_B h_B} \quad (13)$$

A one-center core a valence lone pair (LP)and two-center bond (BD) orbitals are included in a set of Lewis–type NBOs whereas, unoccupied valence nonbonding and extra valence shell Rydberg orbitals as well as the valence antibonding are included in a non -Lewis set. The second-order perturbation approach can be used to obtain the hyperconjugative interaction energy [19].

2.6. UV – VISIBLE SPECTROSCOPY

Ultraviolet-visible spectroscopy is the absorbance of light energy or electromagnetic radiation, that covers 1.5 – 6.2 eV which relates to a wavelength range of 800-200 nm, which excites electrons from the ground state to the first singlet excited state of a material. The wavelength at which the material absorbs the maximum amount of light is known as the absorption maximum,λ_{max}. When the matter absorbs ultraviolet radiation, the electrons undergo excitation causing them to jump from a ground state to an excited state. The difference in the energies of the ground state and the excited state of the electron is always equal to the amount of ultraviolet radiation or visible radiation absorbed by it.

In Absorption spectroscopy, a sample is placed in the path of light and the absorbance of light at each wavelength is measured. In transmission spectroscopy, the sample is placed in a cuvette and the transmitted light at each wavelength is measured.

According to Beer-Lambert law, absorbance is concentration times the molar attenuation coefficient and the path length. Absorbance can be given as:

$$\boldsymbol{A = \varepsilon c l} \tag{14}$$

Where Ais absorbance,ε is the molar attenuation coefficient of the compound or molecule in solution ($M^{-1}cm^{-1}$), the path length is denoted by l and c is the concentration of the solution(M). In the logarithmic function of the ratio of the intensity of the incident light, I_0, to the intensity of transmitted light, I

$$\boldsymbol{A = \log \frac{I_0}{I}} \tag{15}$$

The intensity of an electronic absorption is given by Lambert-Beer law:

$$\boldsymbol{\varepsilon = \frac{1}{cl} \log_{10} \frac{10}{I}} \tag{16}$$

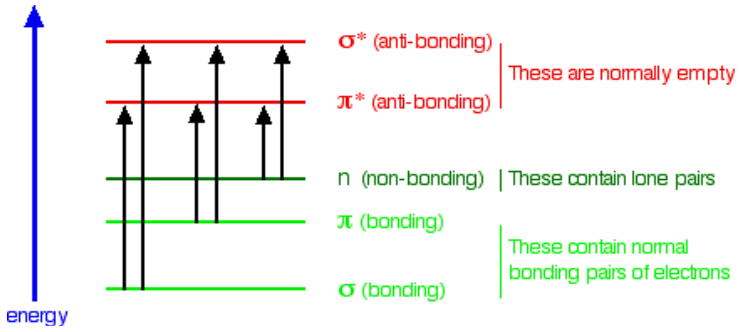

Fig 3. Molecular electronic energy levels (source [3])

UV-visible spectroscopy has a variety of applications including analytical chemistry, biochemistry, environmental science, and pharmaceuticals. It can be used to identify and characterize molecules and to measure the concentration of molecules in solution, to determine the purity of a sample.

In terms of transmittance (T) the beer–Lambert law becomes

$$\boldsymbol{A = -T} \tag{17}$$

Where $\boldsymbol{T = \frac{I}{I_0}}$,

The oscillator strength (f) is given by

$$\boldsymbol{\varepsilon = 0.464 \times 10^9 \frac{f}{\Delta v}} \tag{18}$$

Where Δv is the range of wavenumbers (reciprocal wavelengths) over which the electronic transition extends and f is a measure of the number of electrons per molecule taking part in the transitions responsible for the absorption of light.

2.7. POLARIZABILITY AND HYPERPOLARIZABILITY

Non-linear optics is the study of phenomena in which modification of the optical properties of a material system takes place due to intense light. Laser is a high-intensity source to induce nonlinear optical mechanisms, even in weak nonlinear materials. The induced dipole moment per unit volume is known as electric polarization. To understand nonlinear – optics consider the case when the electric fields are time-independent, where the fields and dipole moments point in the same direction. The dipole moment of a molecule changes when is placed under an electric field i.e.

$$\boldsymbol{p = p_0 + \alpha E + \beta E^2 + \gamma E^3 + \cdots} \tag{19}$$

Where,p_0 is the dipole moment with no field applied,$\alpha$is called the polarizability,$\beta$the hyperpolarizability, $\gamma$the second hyperpolarizability, etc. The linear and nonlinear response is determined by expressing the induced dipole moment as a series in the electric field. As the dipole moment is given as a function of the electric field, P(E), the polarizability and hyperpolarizability can be expressed as

$$\boldsymbol{\alpha = \frac{dp}{dE}} \quad \textbf{and } \boldsymbol{\beta = \frac{1}{2}\frac{\partial \hat{} 2p}{\partial E \hat{} 2}} \tag{20}$$

Second–harmonic generation is a nonlinear optical process in which two photons with the same frequency interact with a nonlinear material, are combined, and generate a new photon with twice

the energy of the initial photons. So the frequency of the new photon is twice the original one. The second harmonic polarization occurs only in certain types of crystals. In isotropic medium 2nd harmonic generation does not occur. Crystals that lack inversion symmetry show 2nd harmonic generation [21].

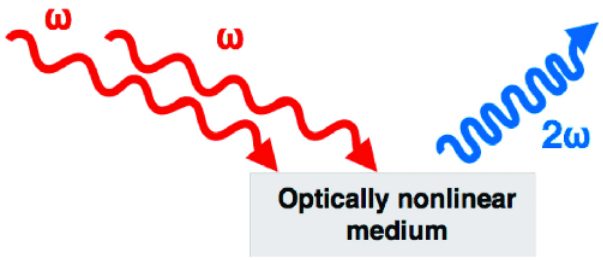

Fig 4. Second harmonic generation

According to classical theory, light scattering arises from oscillations in the charge and current distribution in matter induced by the incident electromagnetic wave. The oscillating electric dipole $\mu(t)$ is linearly related to the electric field strength $E(t) = E_0 \cos \omega t$ of the monochromatic incident wave of angular frequency ω,

$$\boldsymbol{\mu_\alpha(t) = \alpha_{\alpha\beta} E_\beta(t)} \tag{20}$$

The second–rank polar tensor $\alpha_{\alpha\beta}$ is called the polarizability and is a function of ω.T he molecular polarizability tensor $\alpha_{\alpha\beta}$ is normally a symmetric tensor with a maximum of six independent components $(\alpha_{xx}, \alpha_{xy}, \alpha_{xz}, \alpha_{yy}, \alpha_{yz}, \alpha_{zz})$. If the molecule possesses symmetry elements this number may be reduced [21]. Hyperpolarizability is the sum of the nonlinear optical properties of a molecule, is the second-order electric susceptibility per unit volume A nonzero hyperpolarizability indicates a nonlinear response which mean an inflated reaction to the applied field .One such reaction is the second and third harmonic generation where light f frequency ω generates in a material light with frequency 2ω and 3ω respectively[24]. Static polarizabilities are the first response of the electron density to electric fields, and are therefore important for predicting intermolecular and molecule-field interactions. It describes how easily the electron cloud can be deformed under the influence of an external static electric field. When the system is placed in a static electric field, the electronic charge of the system redistributes. This response can be

characterized by induced multipole moments. Of these, the induced dipole moment is related to the static dipole polarizabilities. It measures the change at first order in the molecular dipole moment with the interaction of an external homogeneous electric field [26].

When a strong electric field is applied to a material, the refractive index of the material changes. If the change is linearly proportional to the electric field, the effect is called the Pockel effect. It is proportional to the square of the field, then it is called Kerr effect. In the case of the optical Kerr effect the electric field is the field of the light,so this is the light-induced change of the material refractive index .In particular, the optical Kerr effect is responsible for the self-focusing of the intense laser beams in materials, which is widely used for the self-mode locking in Ti : sapphire lasers , and also known as Kerr lens[27]. The polarization induced in matter by the electric field of an optical wave has a nonlinear component that depends on higher powers of the optical electric field. A second–order response leads to the linear electro-optic (Pockels) effect and to the generation of new optical frequencies through processes such as difference frequency or second harmonic generation [28].

2.7.1. KERR ELECTRO-OPTIC EFFECT (DC KERR EFFECT)

A light beam passing the glass can experience a polarization-dependent change of optical phase which is proportional to the square of the voltage applied to the electrodes i.e., to the square of the electric field strength. The polarization dependence implies that birefringence is induced even in an optical material that is naturally not birefringent. Assuming a constant electric field strength over some path length L, the field–induced phase change is

$$\Delta\boldsymbol{\varphi} = \frac{\mathbf{2\pi}}{\boldsymbol{\lambda}}\boldsymbol{L\Delta n} = \mathbf{2\pi KLE^2} \qquad (21)$$

Where Δn is the difference in refractive index between two polarization directions (parallel and perpendicular to the electric field direction), K is the Kerr constant of the material and E is the applied electric field strength. The Kerr electro-optic effect is generally quite weak compared with the Pockels effect.

2.7.2. Optical Kerr effect (AC Kerr effect)

The Kerr effect occurs without an externally applied electric field, based on the electric field of light only. The Kerr effect is the effect of an instantaneously occurring nonlinear response. The light wave creates a nonlinear polarization wave which acts back on it [30].

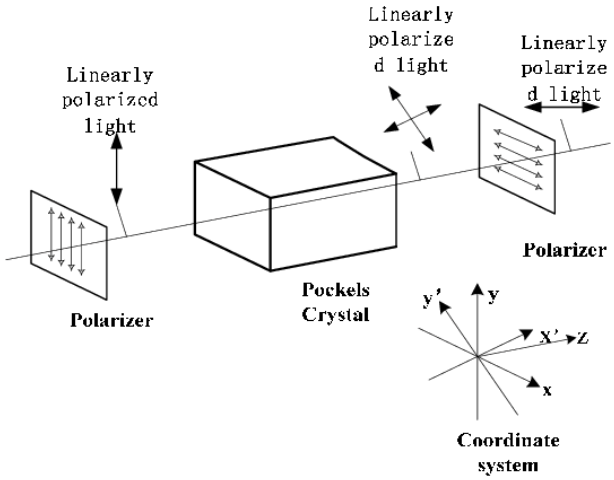

Fig 5: Pockels electro-optic effect

For determining the hyperpolarizability its conversion factor and their corresponding values,

1 a.u.=0.1482 $\times 10^{-24}$ esu for polarizability (α)

1 a.u.=8.6393 $\times 10^{-33}$ esu for first hyperpolarizability (β)

1 a.u = 5.036238$\times 10^{-40}$ esu for second hyperpolarizability (γ)

Some microscopic second-order NLO phenomena at different frequency inputs, second harmonic generation, the process that converts the ω input beam to a 2ω output beam, is the most widely studied ANLO process. The efficiency of this conversion or SHG – activity of a molecule depends on the first hyperpolarizability coefficient $\beta(-2\omega;\omega,\omega)$;reliable measurements of $\beta(-2\omega;\omega,\omega)$ are thus required to study the SHG – activity Commonly used experimental techniques for the determination of molecular first hyperpolarizability are polarizability(α), static first hyperpolarizability ($\beta(o;o,o)$), dynamic first -hyperpolarizabilities ($\beta(-\omega;\omega,o)$ and

$\beta(-2\omega;\omega,\omega)$, static second – hyperpolarizability ($\gamma(0;0,0,0)$), quadratic electro optic Kerr effect ($\gamma(-\omega;\omega,o,o)$) and electric field induced second – harmonic generation ($\gamma(-2\omega;\omega,\omega,0)$).

The isotropic mean polarizability ($<\propto>$), anaisotropy of the polarizability ($\Delta\alpha$) and the total dipole moment (μ_{total}) are defined as

$$<\boldsymbol{\alpha}>=\frac{\mathbf{1}}{\mathbf{3}}(\boldsymbol{\alpha_{xx}}+\boldsymbol{\alpha_{yy}}+\boldsymbol{\alpha_{zz}})$$

$$\Delta\boldsymbol{\alpha}=\frac{\mathbf{1}}{\sqrt{\mathbf{2}}}[(\boldsymbol{\alpha_{xx}}-\boldsymbol{\alpha_{yy}})^{\mathbf{2}}+(\boldsymbol{\alpha_{yy}}-\boldsymbol{\alpha_{zz}})^{\mathbf{2}}+(\boldsymbol{\alpha_{zz}}-\boldsymbol{\alpha_{xx}})^{\mathbf{2}}+\mathbf{6}\boldsymbol{\alpha_{xy}^{2}}+\mathbf{6}\boldsymbol{\alpha_{yz}^{2}}+\mathbf{6}\boldsymbol{\alpha_{xz}^{2}}]^{\mathbf{1/2}} \quad (22)$$

$$\boldsymbol{\mu_{total}}=(\boldsymbol{\mu_{x}^{2}}+\boldsymbol{\mu_{y}^{2}}+\boldsymbol{\mu_{z}^{2}})^{\mathbf{1/2}} \quad (23)$$

The total first – **hyperpolarizability** $(\boldsymbol{\beta_{total}})=(\boldsymbol{\beta_{x}^{2}}+\boldsymbol{\beta_{y}^{2}}+\boldsymbol{\beta_{z}^{2}})^{\mathbf{1/2}}$ (24)

Where,

For $\beta(0;0,0)$:

$$\boldsymbol{\beta_{x}}=\boldsymbol{\beta_{xxx}}+\boldsymbol{\beta_{yxy}}+\boldsymbol{\beta_{zxz}},$$

$$\boldsymbol{\beta_{y}}=\boldsymbol{\beta_{yyy}}+\boldsymbol{\beta_{zyz}}+\boldsymbol{\beta_{xxy}},$$

$$\boldsymbol{\beta_{z}}=\boldsymbol{\beta_{zzz}}+\boldsymbol{\beta_{xxz}}+\boldsymbol{\beta_{yyz}}.$$

For $\beta(-\omega;\omega,0)$:

$$\boldsymbol{\beta_{x}}=\boldsymbol{\beta_{xxx}}+\boldsymbol{\beta_{yyx}}+\boldsymbol{\beta_{zzx}},$$

$$\boldsymbol{\beta_{y}}=\boldsymbol{\beta_{yyy}}+\boldsymbol{\beta_{zzy}}+\boldsymbol{\beta_{yxx}},$$

$$\boldsymbol{\beta_{z}}=\boldsymbol{\beta_{zzz}}+\boldsymbol{\beta_{zxx}}+\boldsymbol{\beta_{zyy}}.$$

And for β(-2$\omega;\omega,\omega$):

$$\boldsymbol{\beta_{x}}=\boldsymbol{\beta_{xxx}}+\boldsymbol{\beta_{xyy}}+\boldsymbol{\beta_{xzz}},$$

$$\boldsymbol{\beta_{y}}=\boldsymbol{\beta_{yyy}}+\boldsymbol{\beta_{yzz}}+\boldsymbol{\beta_{xyx}},$$

$$\boldsymbol{\beta_{z}}=\boldsymbol{\beta_{zzz}}+\boldsymbol{\beta_{xzx}}+\boldsymbol{\beta_{yzy}}$$

The orientationally averaged static second-hyperpolarizability $\gamma(0;0,0,0)$ can be expressed as

$$< \gamma >= \frac{1}{2}(\gamma_{xxxx} + \gamma_{yyyy} + \gamma_{zzzz} + 2\gamma_{xxyy} + 2\gamma_{xxzz} + 2\gamma_{yyzz}) \quad (25)$$

Where the eq. holds the symmetry relations:$\gamma_{xxyy} = \gamma_{yyxx} = \gamma_{xyyx} = \gamma_{yxxy}$.

In the case of the frequency – dependent second hyperpolarizability for the quadratic electro optic Kerr effect where the symmetry relations give $\gamma_{xyyx} = \gamma_{yxyx} = \gamma_{yxxy} = \gamma_{xyxy} \neq \gamma_{xxyy} \neq \gamma_{yyxx}$ the corresponding second – hyperpolarizability is calculated using the equation:

$$\gamma(-\omega; \omega, 0, 0)$$
$$= \frac{1}{5}[\gamma_{xxxx} + \gamma_{yyyy} + \gamma_{zzzz}] + \frac{1}{15}[\gamma_{xxyy} + 4\gamma_{yxyx} + \gamma_{yyxx}]$$
$$+ \frac{1}{15}[\gamma_{xxzz} + 4\gamma_{zxzz} + \gamma_{zzxx}] + \frac{1}{15}[\gamma_{yyzz} + 4\gamma_{zyzy} + \gamma_{zzyy}]$$

The dynamic second hyperpolarizability for the electric – field – induced second – harmonic generation is given by

$$\gamma(2\omega; \omega, \omega, 0)$$
$$= \frac{1}{5}[\gamma_{xxxx} + \gamma_{yyyy} + \gamma_{zzzz}] + \frac{1}{15}[2\gamma_{xxyy} + \gamma_{xyyx} + 2\gamma_{yyxx} + \gamma_{yxxy}]$$
$$+ \frac{1}{15}[2\gamma_{xxzz} + \gamma_{xzzx} + 2\gamma_{zzxx} + \gamma_{zxxz}] + \frac{1}{15}[2\gamma_{yyzz} + \gamma_{yzzy} + 2\gamma_{zzyy}$$
$$+ \gamma_{zyyz}$$

Where the eq. holds the symmetry relations:$\gamma_{xxyy} = \gamma_{xyxy \neq} \gamma_{xyyx}$ [30].

2.8.NON-LINEAR OPTICS

Nonlinear optics is the study of phenomena that occur as a consequence of the modification of the optical properties of a material system by the presence of light. They are nonlinear in the sense that they occur when the response of a material system to an applied optical field depends in a nonlinear manner on the strength of the optical field. The intensity of light generated at the second-harmonic frequency tends to increase as the square of the intensity of the applied laser light.

Consider the polarization P(t), of a material system depends on the strength E(t) of an applied optical field. The induced polarization depends on the electric field strength.

$$\widetilde{\boldsymbol{P}}(\mathbf{t}) = \epsilon_{\mathbf{0}}\, \boldsymbol{\chi}^{(\mathbf{1})}\widetilde{\boldsymbol{E}}(\boldsymbol{t}) \tag{26}$$

Where the constant of proportionality $\chi^1$is known as the linear susceptivity and ε_0 is the permittivity of free space. The polarization $\tilde{P}(t)$ as a power series in the field strength $\tilde{E}(t)$ as

$$\widetilde{\boldsymbol{P}}(\boldsymbol{t}) = \boldsymbol{\varepsilon_0}[\boldsymbol{\chi}^{(\mathbf{1})}\widetilde{\boldsymbol{E}}(\boldsymbol{t}) + \boldsymbol{\chi}^{(\mathbf{2})}\widetilde{\boldsymbol{E}}^{\mathbf{2}}(\boldsymbol{t}) + \boldsymbol{\chi}^{(\mathbf{3})}\widetilde{\boldsymbol{E}}^{\mathbf{3}}(\boldsymbol{t}) \dots \dots \dots \dots]$$

$$\equiv \widetilde{\boldsymbol{P}}^{\mathbf{1}}(\boldsymbol{t}) + \widetilde{\boldsymbol{P}}^{\mathbf{2}}(\boldsymbol{t}) + \widetilde{\boldsymbol{P}}^{\mathbf{3}}(\boldsymbol{t}) \dots \dots \dots$$

The quantities $\chi^{(2)}$and $\chi^{(3)}$

are known as the second and third-order nonlinear optical susceptibilities in which $\tilde{P}^2(t) = \epsilon_0\chi^2\tilde{E}^2(t)$ as the second-order nonlinear polarization and $\tilde{P}^{(3)} = \epsilon_O\chi^{(3)}\widetilde{E^3}(t)$ as the third-order nonlinear polarization [10].

Nonlinear optics has increased applications that include telecommunications, commercial lasers, interaction with materials, and information technology. It brought many technological advances through the study of nonlinear optics in new structures such as quantum wells and optical fibers[11].It describes elastic and inelastic light scattering phenomena and also the behavior of light in nonlinear media, when intense laser light interacts with materials, the intense electric field induces a nonlinear (anharmonic).NLO crystals play an important role in the field of photo electronics, optical communication, optical modulators, laser spectroscopy, frequency conversion and so on.

2.8.1. SECOND HARMONIC GENERATION

A polarization oscillating at frequency 2ω radiates an electromagnetic wave of the same frequency which propagates with the same velocity as that of the incident wave The wave that is produced has the same characteristics of directionality and monochromaticity as the incident wave and is emitted in the same direction .This phenomenon is known as the second harmonic generation. The nonlinear polarizability $\chi^{(2)}$ depends on the direction of propagation, the polarization of the

electric field and the orientation of the optic axis of the crystal. The second-order polarization, therefore may be represented by the relation:

$$\boldsymbol{P_i^{(2)} = \varepsilon_0 \sum_{j,k} \chi_{ijk}^{(2)} E_j E_k} \quad (27)$$

Where i , j, k represent the coordinates x, y ,z. If the second harmonic generation occurs in isotropic crystals.χ_{ijk},is independent of direction and hence it is constant. If it reverses the direction of axis leaving the electric field and dipole moment unchanged in direction, the sign must change,

$$\boldsymbol{-P^{(2)} = \varepsilon_0 \sum_{j,k} \chi_{ijk}^{(2)} \left(-E_j\right)\left(-E_k\right) = +P_i^{(2)}} \quad (28)$$

Which means $P_i^{(2)} = 0$ and hence,$\chi_{ijk}^{(2)} = 0$

Second harmonic generation therefore cannot occur in isotropic medium, such as liquids or gases nor in centro-symmetric crystals. Crystals that lack inversion symmetry exhibit SHM. Therefore, it can be written as [13].

$$\boldsymbol{P = \varepsilon_0 \chi^{(1)} E + \varepsilon_0 \chi^{(2)} E^2} \quad (29)$$

Consider the optical field incident upon a second–order nonlinear optical medium, which consists of two distinct frequency components in the form,

$$\boldsymbol{\widetilde{E}(t) = E_1 e^{-i\omega_1 t} + E_2 e^{-i\omega_2 t} + c.c.} \quad (30)$$

The second–order contribution to the nonlinear polarization is given by

$$\boldsymbol{\widetilde{P}^{(2)}(t) = \varepsilon_0 \chi^{(2)}\left[E_1^2 e^{-2i\omega_1 t} + E_2^2 e^{-2i\omega_2 t} + 2E_1 E_2 e^{-i(\omega_1+\omega_2)t} + 2E_1 E_2^* e^{-i(\omega_1-\omega_2)t} + c.c.\right] + 2\varepsilon_0 \chi^{(2)}[E_1 E_1^* + E_2 E_2^*]} \quad (31)$$

The complex amplitudes of the various frequency components of the nonlinear polarization are given by

$P(2\omega_1) = \varepsilon_0 \chi^{(2)} E_1^2$ (Second harmonic generation),

$P(2\omega_2) = \varepsilon_0 \chi^{(2)} E_2^2$(Second harmonic generation),

$P(\omega_1 + \omega_2) = 2\varepsilon_0 \chi^{(2)} E_1 E_2$(Sum-Frequency generation)

$P(\omega_1 - \omega_2) = 2\varepsilon_0\chi^{(2)}E_1E_2^*$(Difference-Frequency generation)

$P(0) = 2\varepsilon_0\chi^{(2)}(E_1E_1^* + E_2E_2^*)$(Optical rectification)

The four different nonzero frequency components are present in the nonlinear polarization. No more than one of these frequency components will be present with any intensity in the radiation generated by the nonlinear optical interaction.

2.8.2. TWO-PHOTON PROCESSES

A coherent light wave with frequency ω transforms into a coherent light wave of another frequency cannot take place through the direct interaction between two photons. The transformation of photons can be brought about only through an intermediary quantum system such as an atom or molecule characterized by a system of discrete energy levels. An atom or a molecule can absorb or emit photons and, in the process, they may undergo a transition from one energy level to the other.

Consider an atom absorbs energy $h\omega$ and changes from level 1 to level 2. After a short while, it returns to level 1 by emitting a photon of the same energy. The state of the atom remains unaltered but the emitted photon although has the same energy as the incident photon, may be in a different state with different momentum, direction, and polarization. Thus, the atom has acted in this transformation as an intermediary.

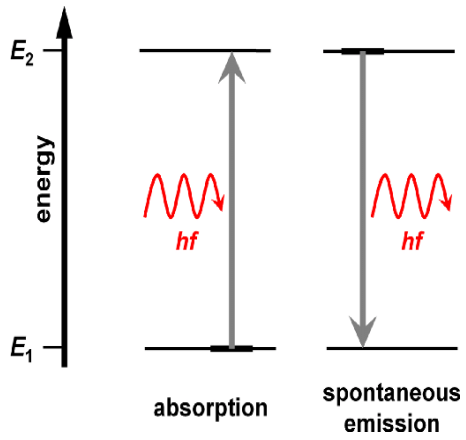

Fig 6: Energy diagram of two photon process (source[4])

Consider another process in which the molecule absorbs a photon of energy $\hbar\omega_{13}$ and shifts from level 1 to level 3 and then emits a photon of energy $\hbar\omega_{32}$ by dropping from level 3 to level 2 .so the frequency is converted through an intermediary role played by the molecule.

Consider the third–order contribution to the nonlinear polarization

$$\widetilde{\boldsymbol{P}}^{(3)}(\boldsymbol{t}) = \boldsymbol{\varepsilon_0}\boldsymbol{\chi}^{(3)}\widetilde{\boldsymbol{E}}(\boldsymbol{t})^{3} \tag{33}$$

When the applied field is monochromatic and is given by

$$\widetilde{\boldsymbol{E}}(\boldsymbol{t}) = \boldsymbol{\varepsilon}\,\boldsymbol{cos\omega t} \tag{34}$$

We can express the nonlinear polarization as

$$\widetilde{\boldsymbol{P}}^{(3)}(\boldsymbol{t}) = \frac{\boldsymbol{1}}{\boldsymbol{4}}\boldsymbol{\varepsilon_0}\boldsymbol{\chi}^{(3)}\boldsymbol{\varepsilon}^{3}\boldsymbol{cos3\omega t} + \frac{\boldsymbol{3}}{\boldsymbol{4}}\boldsymbol{\varepsilon_0}\boldsymbol{\chi}^{(3)}\boldsymbol{\varepsilon}^{3}\boldsymbol{cos\omega t} \tag{35}$$

The first term describes a response at frequency 3ω that is created by an applied field at a frequency ω.This term leads to the process of third harmonic generation.

CHAPTER 3

MATERIALS AND METHODS

3.1. Synthesis

Pour 15 milliliters of methanol into a beaker and dissolve Co (NO3)2.6H2O at a mass of 0.4365g (0.1 molarity). In another beaker, dissolve approximately 0.142 g of 0.1 molarity pyridine N-oxide in 15 ml of methanol. Pour drop by drop of pyridine N-oxide solution into Co (NO3)2.6H2O solution and stir for 45 minutes. The solution has turned a light crimson colour. Upon 140 days of gradual evaporation, Figure 2 depicts the thin crimson colour block shape crystals known as Di aqua bis (nitrato)-bis(1λ5-pyridin-1-olato)-cobalt.

3.2. Crystal structure determination

The X-ray intensity data were measured (λ = 0.71073 Å) under three hours of exposure of the sample. A narrow-frame technique was used to combine the frames with the Bruker SAINT software suite. A maximum θ angle of 28.582 degrees was obtained by integrating the data with a triclinic unit cell, resulting in 9222 reflections in total (0.75 Å resolution). The final cell constants and volume were derived from the 1888 reflections above 20 σ(I) XYZ-centroids that have been refined to have 7.114 ° < 2θ < 57.164°. The crystal structure is displayed in Figure 2 and the CIF has been deposited in CCDC under CIF no. 2266302. Table 1 provides specifics of the crystal and refinement data. SHELXL97 (Sheldrick, 2008), ORTEP-3 (Farrugia, 1997), APEX2 (Bruker, 2004), APEX2/SAINT (Bruker, 2004), SAINT/XPREP (Bruker, 2004), SIR92 (Alternate et al., 2014), and Mercury (Bruno et al., 2002) computer programs were used to determine single crystal XRD.

3.3. THEORETICAL CALCULATIONS

The crystal is made and optimized by computation in the workstation. It has been confirmed that Diasquabis (nitrato)-bis(1λ5-pyridine-1-olato)-cobalt. The program has been run by Gaussian G09 one calculated using the b3LYP/def2TZVP/LANL2DZ mixed basis set level of theory, optimization is the stable and minimum position, which shows all characteristic properties of a molecule. The output comes from the origin analysis software used to draw the diagrams. With the help of other software such as Origin, Chem craft, Multifwn, the computation was done. Chem craft is used to calculate bond length and bond angle. Multifwn was used to extract the hyperpolarizability values from Gaussian. Hirshfield analysis is done by crystal Explorer 21.5 helped to investigate different types of intermolecular interactions. It is analyzed and done using Chemcraft.

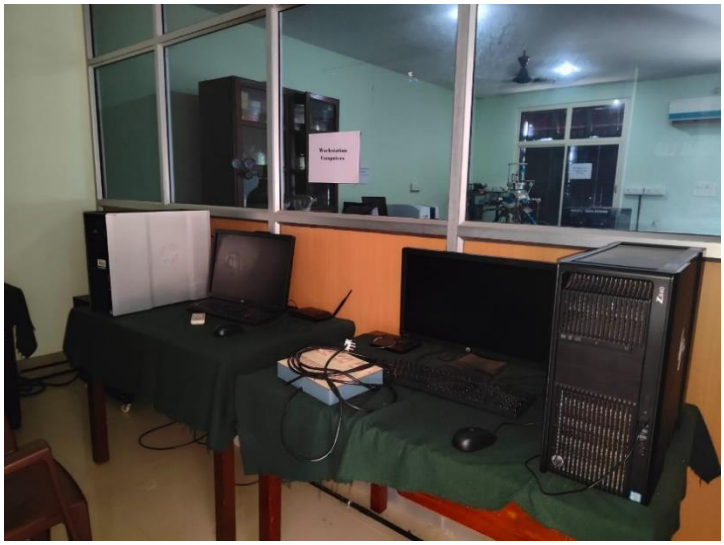

Figure 7: DFT Workstation

The natural bond orbital analysis provides information about the interaction in both filled and virtual orbitals and can be used for the investigation of intra- and intermolecular interactions. NBO analysis of the Diasquabis(nitrato)-bis(1λ5-pyridine-1-olato)-cobalt has been carried out at the

b3LYP/def2TZVP/LANL2DZ level of theory. To evaluate the donor-acceptor contacts, the second-order Fock matrix has been calculated.

The vibrational assignments were done at b3LYP/defT2ZVP/LANL2DZ level and stimulated IR spectra were studied, from this we can find about the strength of the system from the study of bond length and bond strength of the molecules and can also find the presence of atoms in the compound. The infrared spectrum is studied by Gauss view and the graph that is plotted in terms of transmittance is done in origin software.

The hyperpolarizability was calculated by Gaussian G09 software. In the presence of an applied electric field, the energy of a system is a function of the electric field. The important parameters of hyperpolarizability are used to find donor-acceptor systems, nature of substituents, influence of planarity. The hyperpolarizability values are extracted with the help of multifwn software.

CHAPTER 4

RESULT AND DISCUSSION

4.1 OPTIMIZED GEOMETRIC PARAMETERS

The bond length of Diaquabis(nitrato)(1λ5-pyridine-1-olato)-cobalt was analyzed from the output of optimized geometry with B3LYP/def2TVZP/LANL3DZ level.

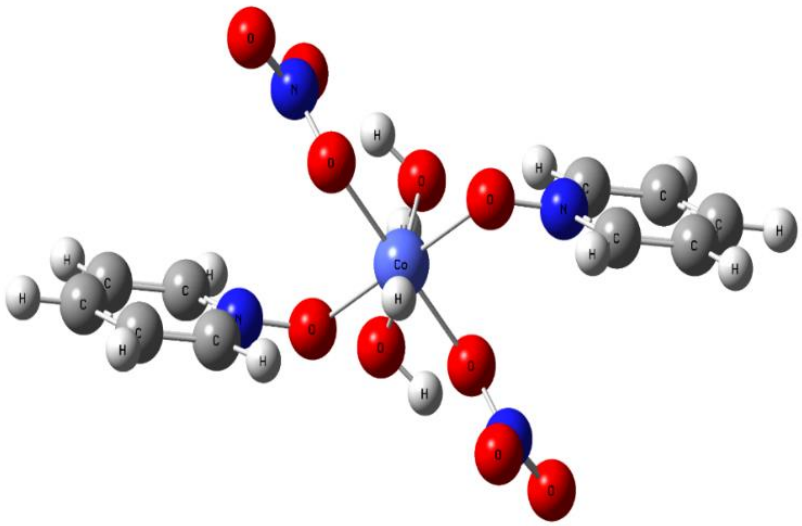

Fig 7. Optimized geometry of Diaquabis (nitrato)-bis(1λ5-pyridine-1-olato)-cobalt at B3LYP/def2TZVP/LANL2DZ level of theory

The bond length and bond angle of the title compound are tabulated in Table 1. We get very good accuracy.

BOND LENGTH (A^0)	b3lyp	X-ray	BOND ANGLES (0)	B3lyp	X-ray
C_{23}-C_{25}	1.389	1.366	H_2-C_1-C_3	125.1	120.3
C_{25}-H_{26}	1.081	0.93	H_2-C_1-N_{11}	115	120.2
C_{25}-C_{27}	1.39	1.367	C_3-C_1-N_{11}	120	119.6
C_{27}-H_{28}	1.081	0.931	C_1-C_3-H_4	118.3	120
C_{27}-C_{29}	1.378	1.362	C_1-C_3-C_5	120.3	119.8
C_{29}-H_{30}	1.078	0.93	C_1-N_{11}-C_9	120.8	121.6
C_{29}-N_{31}	1.355	1.333	C_1-N_{11}-O_{13}	120.9	119.3
N_{31}-O_{33}	1.323	1.347	H_4-C_3-C_5	121.4	120.2
N_{32}-O_{35}	1.299	1.267	C_3-C_5-H_6	120.8	120.4
N_{32}-O_{36}	1.218	1.216	C_3-C_5-C_7	118.5	119.2
N_{32}-O_{37}	1.258	1.241	H_6-C_5-C_7	120.7	120.4
O_{34}-H_{38}	0.989	0.842	C_5-C_7-H_8	121.5	120
O_{34}-H_{39}	0.965	0.838	C_5-C_7-C_9	119.8	120
			H_8-C_7-C_9	118.7	120

Table 1. Optimized geometric parameters

Optimized geometric parameters i.e. bond angle with theoretical and X-ray values

ANGLES (0)	b3lyp	X-ray

C7-C9-H10	124.8	120
C7-C9-N11	120.6	119.9
H10-C9-N11	114.6	120.1
C9-N11-O13	118.3	119.1
N11-O13-Co18	122.4	120.1
O15-N12-O16	118.3	118.4
O15-N12-O17	119.4	119.9
N12-O15-Co18	128.2	131.3
O16-N12-O17	122.3	121.7
O13-Co18-O14	95.7	89.7
O13-Co18-O15	92.6	94.4
O13-Co18-O33	180	180
O13-Co18-O34	84.3	90.3
O13-Co18-O35	87.4	85.6
Co_{18}-O_{14}-H_{19}	92.2	95.9
Co_{18}-O_{14}-H_{20}	100.8	128.1
O_{14}-Co_{18}-O_{15}	83.2	86.4
O_{14}-Co_{18}-O_{33}	84.3	90.3
O_{14}-Co_{18}-O_{34}	180	180
O_{14}-Co_{18}-O_{35}	96.8	93.6
H_{19}-O_{14}-H_{20}	107.2	110.9
O_{15}-Co_{18}-O_{33}	87.4	85.6
O_{15}-Co_{18}-O_{34}	96.8	93.6

O_{15}-Co_{18}-O_{35}	180	180
O_{33}-Co_{18}-O_{34}	95.7	89.7
O_{33}-Co_{18}-O_{35}	92.6	94.4
Co_{18}-O_{33}-N_{31}	122.4	120.1
O_{34}-Co_{18}-O_{35}	83.2	86.4
Co_{18}-O_{34}-H_{39}	92.2	95.9
Co_{18}-O_{35}-N_{32}	100.8	128.1
H_{22}-C_{21}-C_{23}	128.2	131.3
H_{22}-C_{21}-N_{31}	125.1	120.2
C_{23}-C_{21}-N_{31}	115	120.2
C_{21}-C_{23}-H_{24}	120	119.6
C_{21}-C_{23}-C_{25}	118.3	120
C_{21}-C_{23}-H_{25}	120.3	119.3
C_{21}-N_{31}-C_{29}	120.8	120.2
C_{21}-N_{31}-O_{33}	120.9	120.4
H_{24}-C_{23}-C_{25}	121.4	119.2
C_{23}-C_{25}-H_{26}	120.8	120.4
C_{23}-C_{25}-C_{27}	118.5	119.2
H_{26}-C_{25}-C_{27}	120.7	120.4
C_{25}-C_{27}-H_{28}	121.5	120
C_{25}-C_{27}-C_{29}	119.8	120
H_{28}-C_{27}-C_{29}	118.7	120.
C_{27}-C_{29}-H_{30}	124.8	120

C_{27}-C_{29}-N_{31}	120.6	119.9
H_{30}-C_{29}-N_{31}	114.6	120.1
C_{29}-N_{31}-O_{33}	118.3	119.1
O_{35}-N_{32}-O_{36}	118.3	118.4
O_{35}-N_{32}-O_{37}	119.4	119.9
O_{36}-N_{32}-O_{37}	122.3	121.7
H_{38}-O_{34}-H_{39}	107.2	110.9

Table 2. Optimized geometric parameters of Diaquabis(nitrato) (1λ5 pyridine-1-olato)-cobalt

Using the value of Table 1, regression analysis was done and figured in Fig 8.

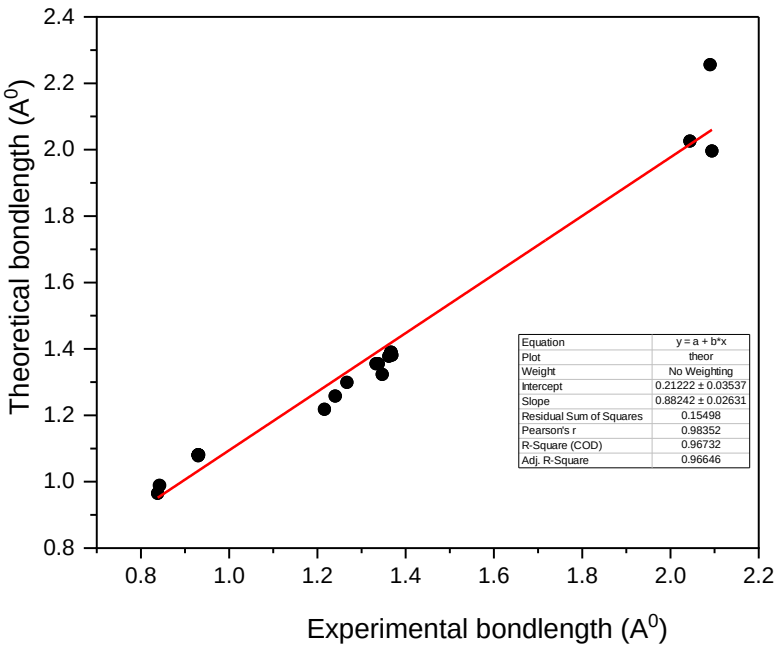

Figure 8: Bond length of diaquabis (nitrato)-(bispyridine-1-olato) cobalt

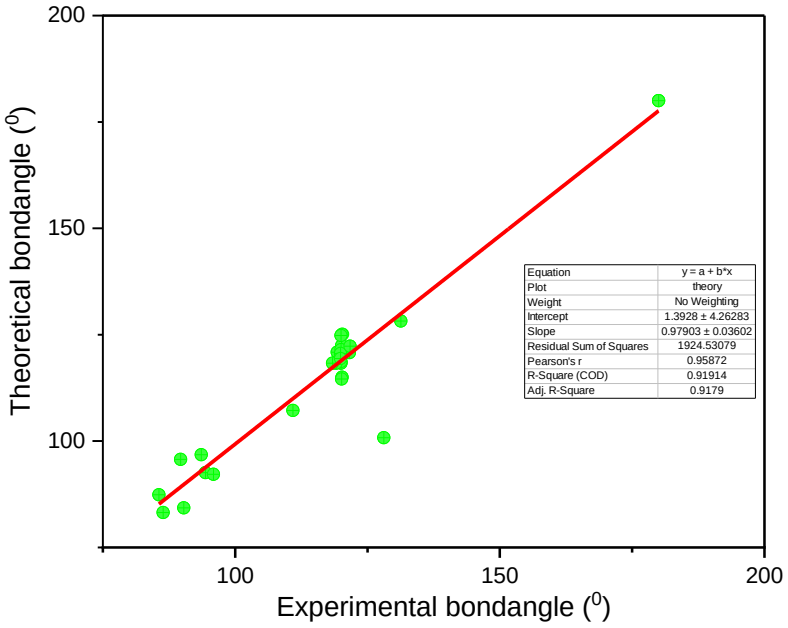

Figure 9: Linear regression of bond parameters of Diaquabis(nitrato)-bis(1λ5-pyridine-1-olato)-cobalt

The optimized structural parameters calculated using the b3lyp/def2TZVP/LANL2DZ basis set are listed in table along with experimental data, corresponding with the atom numbering scheme in fig. The angle H_{30}-C_{29}-N_{31} is increased by $6.5^0$from the theory. The increase in the angle of H_2-C_1-C_3 is increased by $5.2^0$and the angle between experimental and theory of H_{22}-C_{21}-N_{31} is $4.9^0$and that of Co_{18}-O_{18}-N_{32} is 28.7^0. The bond angle is increased to 5.2^0 in C_{23}-C_{21}-N_{31}. The parameters obtained from the computation are found to be comparable with data as understood from the linear regression analysis shown in fig, with values of R^2 is 0.9673, 0.9194 for the fit of bond lengths, and bond angles respectively, and the optimized structure is shown in fig.

4.2 NATURAL BOND ANALYSIS

Donor(i)	ED(i) [e]	Acceptor(j)	ED(j) [e]	E (2) [kcal/mol]	E(j)-E(i) [a.u.]	F (i, j) [a.u.]
$\pi^*(C_9 - N_{11})$	0.27541	$\pi^*(C_5 - C_7)$	0.16150	30.90	0.07	0.088
$n(3)(O_{15})$	0.85374	$\sigma^*(N_{12} - 0_{16})$	0.03099	38.78	0.17	0.113
$n(3)(O_{17})$	0.80921	$\sigma^*(N_{12} - O_{16})$	0.03099	56.58	0.15	0.126
$\pi^*(C_{29} - N_{31})$	0.88217	$\pi^*(C_{25} - C_{27})$	0.81249	30.90	0.07	0.088
$n(3)(O_{35)})$	0.85375	$\sigma^*(N_{32} - O_{36})$	0.99840	38.78	0.17	0.113
$n(3)(O_{37})$	0.80920	$\sigma^*(N_{32} - O_{36})$	0.99840	56.57	0.15	0.126
$n(2)(O_{36})$	0.93937	$\sigma^*(N_{32} - O_{35})$	0.99624	11.22	0.55	0.099
$n(2)(O_{35})$	0.88510	$n^*(8)(Co_{18})$	0.07477	13.98	0.74	0.131
$\pi^*(C_5 - C_7)$	0.16150	$\pi^*(C_9 - N_{11})$	0.27541	17.56	0.21	0.080
$\pi^*(C_9 - N_{11})$	0.27541	$\pi^*(C_1 - C_3)$	0.13832	16.45	0.07	0.067
$n(2)(O_{35})$	0.88510	$n^*(4)Co_{18}$	0.21103	14.30	0.40	0.101
$n(1)(O_{15})$	0.96910	$n^*(8)(Co_{18})$	0.07566	11.19	0.82	0.124
$n(2)(0_{15})$	0.88510	$n^*(5)(Co_{18})$	0.12073	16.51	0.60	0.126
$n(2)(O_{15)}$	0.88519	$n^*(8)(Co_{18})$	0.07477	13.98	0.74	0.131
$n(2)(O_{34})$	0.93600	$n^*(6)Co_{18}$	0.09288	14.41	0.49	0.107
$n(2)O_{34}$	0.93600	$n^*(9)Co_{18}$	0.06721	11.25	0.61	0.105
$\pi(C_{29} - N_{31})$	0.27541	$\pi^*(C_{21} - C_{23})$	0.13832	9.41	0.38	0.076
$\pi(C_{21} - C_{23)}$	0.00701	$\pi^*(C_{25} - C_{27})$	0.16150	10.44	0.28	0.069
$n(3)O_{33}$	0.85670	$n^*(5)CO_{18}$	0.12073	15.00	0.45	0.105

Table 2 : Second-order Fock matric in natural bond orbital basis

The second–order Fock matrix was carried out to evaluate the donor-acceptor interactions in the NBO analysis. The interactions result in a loss of occupancy from the localized NBO of the idealized Lewis structure into an empty non-Lewis orbital. For each donor (i) and acceptor (j), the stabilization energy E (2) associated with the delocalization i→ j is estimated as,

$$E_2 = \Delta E_{ij} = q_i \frac{F(i,j)^2}{\varepsilon_j - \varepsilon_i} \quad (37)$$

Where q_i is the donor orbital occupancy, are $\varepsilon_i \; and \; \varepsilon_j$ diagonal elements, and F(i,j) is the off – diagonal NBO Fock matrix elements. NBO provides a series of second – order perturbation energies E (2) that corresponds to the energetic consequence of the transfer of charge from one orbital of the first molecule to another orbital of the second [19]. The larger the E(2)value, the more intensive the interaction between electron donors and electron acceptors,i.e. the more donating tendency from electron donors to electron acceptors and the greater the extent of conjugation of the whole system.

In the ring,$\pi^*(C_9 - N_{11})$ bond conjugate with,$\pi^*(c_5 - c_7)$ reveals strong delocalization leading to a stabilization energy of 30.90 kcal/mol. The $n(3)O_{15}$ bond conjugates with $\pi^*(N_{12} - O_{16})$ resulting in the stabilization energy of 38.78 kcal/mol. The $n(3)O_{17}$ bond further conjugates with $\pi^*(N_{12} - O_{16})$ supplying an additional energy of 56.58 kcal/mol .The electron donation from $\pi^*(C_{29} - N_{31})$ to the antibonding acceptor $\pi^*(C_{25} - C_{27})$,which leads to a stabilization energy of 30.90 kcal/mol .The lone pair interaction of $n(3)O_{35}$ and $n(3)O_{37}$ with $\sigma^*(N_{32} - O_{36})$ resulting in an energy E(2) of 38.78 kcal/mol and 56.57 kcal/mol respectively. The lone pair interactions of $n(2)O_{35} \longrightarrow n^*(4)Co_{18}$, $n(1)O_{15} \rightarrow n^*(8)Co_{18}$,$n(2)O_{15} \rightarrow n^*(5)Co_{18}$ and $n(2)O_{15} \rightarrow n^*(8)Co_{18}$ are 14.30 kcal/mol,11.19 kcal/mol,16.51 kcal/mol and 13.98 kcal/mol respectively .The stabilization energy of donor $\pi(C_{29} - N_{31})$ with acceptor as $\pi^*(C_{21} - C_{23})$ of 9.41 kcal/mol. $\pi^* C_5 - C_7$ conjugates with$\pi^*(c_9 - N_{11})$ with a stabilization energy of 17.56 kcal/mol. The electron donor from $\pi^*(C_9 - N_{11})$ to the acceptor $\pi^*(C_1 - C_3)$ with energy 16.45 kcal/mol .Electron from $\pi(C_{21} - C_{23})$ to $\pi^*(C_{25} - C_{27})$ with a stabilization energy of 10.44kcal/mol .The lone pair interaction of $n(3)O_{33}$ to $n^*(5)Co_{18}$ with an energy of 15 kcal/mol.

4.3 VIBRATIONAL SPECTRAL ANALYSIS

Vibrational spectroscopy is a spectroscopic method of identifying and classifying compounds based on the vibrations of their bonds .Depending on the type , vibrational spectroscopy either measures which frequencies of radiation are absorbed vs. transmitted .The fingerprint region of a vibrational spectroscopy output refers to a set of vibrations produced by a molecule due to the vibrations of its bonds .Theoretical FT-IR spectra can be obtained through computational methods, such as density functional theory (DFT) calculations ,which can stimulate the vibrational modes and corresponding frequencies of a molecule.

A visual comparison of the stimulated IR and experimental IR spectra is dissipated. Vibrational assignments of the title compound were performed at def2TZVP/LANL2DZ level of theory.

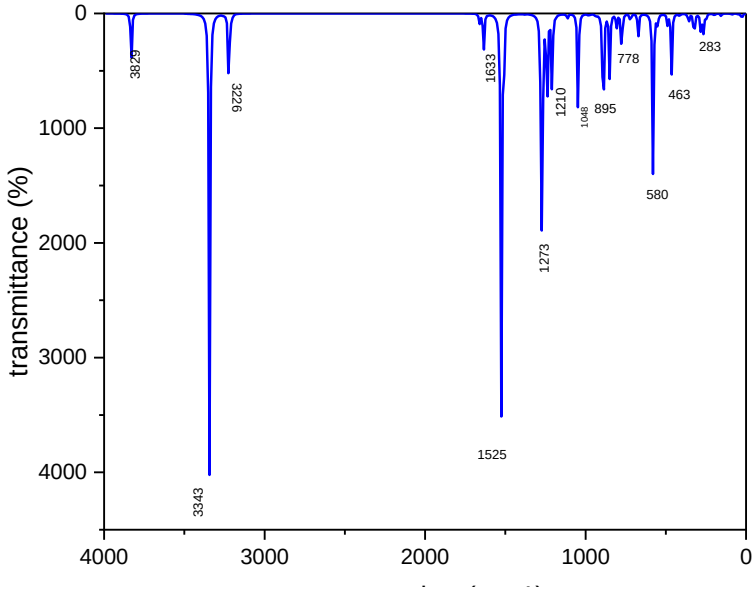

Figure 10: Vibrational spectra of Diaquabis(nitrato)bis (1λ5-pyridine-1-olato) cobalt

Thepeakat3820cm1 corresponds to week stretching vibration. The strong peak corresponds to 3343cm^{-1} is O-H stretching indicates the presence of a hydroxyl group. The presence of weak transmittance peak at 1650 cm^{-1}which is assigned to C=O stretching vibration. The peak in the range of 3300-3350 cm-1 corresponds to O-H stretching which has medium intensity [22] . The

peak in the range of 1515-1560 cm-1 leads to nitro group (N-O) which is a strong bond. The peak at 1273 cm^{-1} is C≡N stretching which is strong. The peak corresponding to 1210cm^{-1} is the C-O stretch [23] . The weak peaks at 778 cm^{-1},553 cm^{-1} are in good agreement with 283 cm^{-1} in stimulated IR spectra. Normally, C-H bending vibrations occur in a region 1000-750 which are at a weak band.

4.4 Hershfeld surface analysis

The Hershfield Surface's various features, including d_{norm}, curvedness, shape index, etc make it valuable for studying intermolecular interactions. The built-in quantum chemistry software TONTO in Crystal Explorer 21.5 is used to simulate surface characteristics.(Tan *et al.*, 2019). The electrostatic potential surface of d_{norm}, shape index, and curvedness of compound 1 is mapped across the Hershfield surface in the following ranges: -0.6536 to 1.0733A0, -1 to 1A0, and -4 to 0.4A0. The distinct circular mark on Figure 7 in d_{norm} surface is caused by H--O interactions, whereas the other red spots on the side view are caused by H--H interactions with neighboring molecules. Additionally, it displays red and blue triangular shapes within the same shape index curve, providing proof of π – π molecular stacking. As we can see, the curvedness graph's flat sections correlate to the red spots and the triangle-shaped regions, supporting the π-π stacking theory. Surface geometry measurements, such as curvedness and shape index, provide fundamental insights into donor-acceptor interactions and π-π stacking. The curvedness graph demonstrates a flat zone in the complex metal-ligand region, indicating π-π stacking. The core metal atom and the blue region that acts as a donor are visible in the shape index >1. An acceptor is a red area with a shape index < 1. Red areas represent acceptor (negative) atoms, and blue sections represent donor (positive) atoms. Longer intermolecular contacts (blue) and shorter intermolecular interactions (red) are produced by these charge interactions. The blue region represents long-range interactions of carbon, and cobalt atoms while short-range interactions (red region) are produced by the oxygen atom (Seth, 2018).

The fingerprint plot highlights the contributions to intermolecular and interatomic interactions made by all pairs of molecules as well as by each pair of atoms. Fingerprint plots allow

us to visualize these interactions. Table 3 displays the range of interactions that are available in the compound. The H · · · O interactions in the compound show up as spikes in Figure 5 (b) and this interaction contributes more, accounting for 59.22% of all interactions. The total of the exterior and interior interatomic distances (de + di ≈ 1.75 A0) showed that crystal can form a two-dimensional network to form the π-π stacking interactions that are produced by these kinds of interactions. Figure 5 (c) illustrates another interaction supplied by H - - H (20.5%), which dispersed and propagated up to de = di = 2.6 A0. The crystal packing is strengthened by the effective hydrogen bondings. C - - H (13.1 %) is another sort of significant interaction; fig. 10(d) depicts a dumble -like dispersed diagram of this interaction. The de + di = 3.25 A^0 is the effective contact distance. Over 3.4% of the surface is covered by the H-N interaction, 2.2% by the C-O interaction, and 0.6% by the O-O interaction.

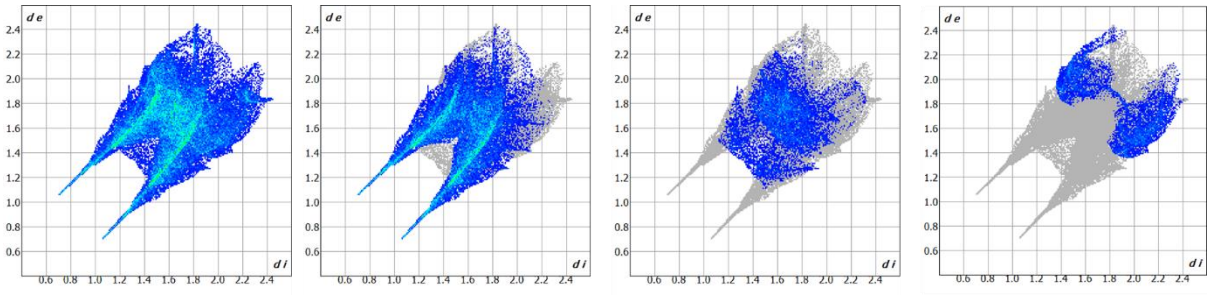

Fig11: Fingerprint plots for close contacts of compound 2 for(a)all contacts (b)H- -O (c) H- -H (d) C- -H

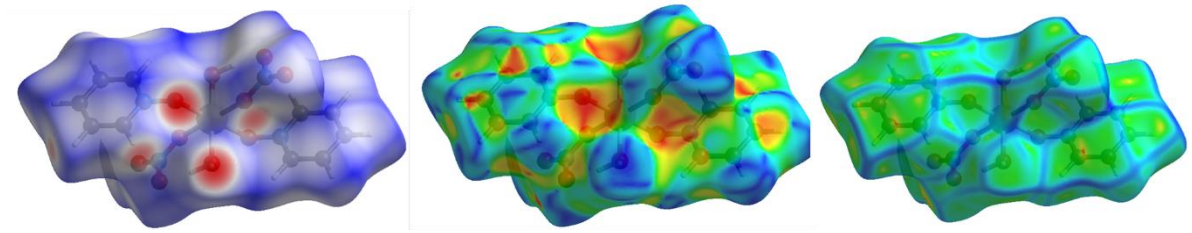

FIGURE 12: Hershfield surface mapped over compound 2 for (a)d_{norm}, (b)shape index (c)curvedness

4.5 HYPERPOLARIZABILITY

The dipole moment, static polarizability, and Dynamic polarizability of diaquabis nitrato(bis pyridine-1-olato)cobalt of basis set b3lyp are calculated. Nonlinear optical (NLO) effects can be measured using first-order hyperpolarizability. The polarizabilities and even more the hyperpolarizabilities are difficult quantities to predict, so they are ideal targets when elaborating new calculation methods. Vibrational versus electronic contributions, frequency dispersion including resonance, electron correction, and relativistic effects, and the impact of the surroundings. On the other hand, linear and nonlinear responses are evaluated [31]. It is known that α is a linear property of the material, defined as the tendency of the material to acquire an electric dipole moment in proportion to an applied electric field. The average polarizability is calculated as the average of the diagonal components of the polarizability tensor. As the volume occupied by the electrons increases, the polarizability should generally increase. This is because the electrons in a larger atom are loosely bound to those in a smaller atom.

NLO coefficient	Diaquabis nitrato bis(1λ5-pyridine-1-olato) cobalt		Urea	Bis(dithiolydene)-tetrathiapentalene(BDT-TTP)
$\mu_{total}(\times 10^{-21}$esu)	1.224747		3.432 Debye	1.8731 D
$\alpha(0,0) \times 10^{-23}$esu	$\alpha\ total$	3.270375	4.942×10^{-24}	30.0122×10^{-24}
	$\Delta\alpha$	2.109322	0.689×10^{-24}	4.4478×10^{-24}
$\alpha(-\omega,\omega) \times 10^{-23}$esu	$\alpha total$	3.510448	4.995×10^{-24}	……..
	$\Delta\alpha$	2.492123	0.682×10^{-24}	……..
$\beta(0;0,0) \times 10^{-34}$esu	4.824848		0.756×10^{-30}	168.8291×10^{-33}
$\beta(-\omega;\omega,0) \times 10^{-33}$esu	1.043618		0.922×10^{-30}	……..

$\beta(-2\omega;\omega,\omega)\times 10^{-31}$esu	6.927662	1.74×10^{-30}	……..
$\gamma(0;0,0,0)\times 10^{-35}$esu	1.832166	4.023×10^{-36}	……..
$\gamma(-\omega;\omega,0,0)\times 10^{-35}$esu	3.388280	5.312×10^{-36}	…….
$\gamma(-2\omega;\omega,\omega,0)\times 10^{-33}esu$	8.964510	7.812×10^{-36}	……..

Table 3: Hyperpolarizability values of the title compound with comparison with urea and BTD

Polarizabilities and hyperpolarizabilities characterize the response of a system in an applied electric field. It determines not only the strength of molecular interactions but also the cross sections of different scattering and collision processes, as well as the NLO properties of the system. The dipole moment, polarizabilities and hyperpolarizabilities characterize the response of a system in an applied electric field. Electric polarizability is a fundamental characteristic of atomic and molecular system. Electric dipole moment, molecular polarizability and anisotropy of polarizability, molecular first hyperpolarizability and second hyperpolarizabilities are investigated. The total static dipole moment μ is calculated as

$$\boldsymbol{\mu_{total} = (\mu_x^2 + \mu_y^2 + \mu_z^2)^{1/2}} \quad (38)$$

The calculated dipole moment is $1.224747\times 10^{-21}esu$ while that of urea and bis (dithiolydene)-tetra thiapentalene are 3.432 and 1.8731 debye respectively. The magnitude of first static polarizability x, y, z component of polarizability is calculated as

$$\boldsymbol{\alpha_{total} = (\alpha_x^2 + \alpha_y^2 + \alpha_z^2)^{1/2}}$$

The calculated polarizability is $3.27035\times 10^{-23}esu$ .while urea and BTD contains 4.942 $\times 10^{-24}$esu and 30.12×10^{-24} esu.The anisotropic polarizability is calculated by the equation:

$$\boldsymbol{\Delta\alpha = \frac{1}{\sqrt{2}}\left[(\alpha_{xx}-\alpha_{yy})^2 + (\alpha_{yy}-\alpha_{zz})^2 + (\alpha_{zz}-\alpha_{xx})^2 + 6\alpha_{xy}^2 + 6\alpha_{yz}^2 + 6\alpha_{xz}^2\right]^{1/2}}$$

The calculated anisotropic polarizability is 2.190322× $10^{-23} esu$.The static polarizability constant β can be evaluated by the equation:

$$\boldsymbol{\beta_{total} = (\beta_x^2 + \beta_y^2 + \beta_z^2)^{1/2}}$$

In which β is calculated and got a value of 4.8248× 10^{-34}esu, and that of dynamic polarizability with coordinates $(-\omega; \omega, 0)$,which is also known as dc-Pockels, has the value of 1.043618× 10^{-33}esu. The SHG, coordinates in the range of $(-2\omega; \omega, \omega)$ is 6.927662× 10^{-31}esu.The polarizability coefficient γ can be calculated by the equation:

$$\boldsymbol{\gamma_{total} = (\gamma_x^2 + \gamma_y^2 + \gamma_z^2)^{1/2}}$$

The value of $\gamma(0; 0,0)$ is 6.927662× 10^{-31}esu that of urea is 4.023× 10^{-36}esu. The value for the coordinates $(-\omega; \omega, 0,0)$ is known as Electro-optic Kerr effect, is 3.388280× 10^{-35}esu. The value for $\gamma(-2\omega; \omega, 0,0)$ is 8.964510× 10^{-33}esu which is known as SHG.

CHAPTER 6

CONCLUSION AND FUTURE SCOPE

6.1. CONCLUSION

The metal-organic crystal Diaquabis(nitrato)-bis (1λ5-pyridine -1-olato)-cobalt has been synthesized by a slow evaporation method and crystal structure was confirmed. The crystal structure has been optimized using Gaussian software at the b3LYP/def2TVP/LANL2DZ level correctly because of the high-level basis set and function. The value of R^2 obtained is 0.919. We get a global minimum and there is no imaginary frequency found. The NBO analysis reveals the strong charge interaction and stabilization of molecules. The nonlinearity of Diaquabis (nitrato)-bis (1λ5-pyridine 1-olato)-cobalt provided from the strong electron delocalization nitroyl and aqua compounds center cobalt to ligand charge transfer. By this study, we can explore the charge interaction. The vibrational spectra analysis of the compound is theoretically proved. The strong and weak stretching modes of vibrations of different groups in this compound is determined with the help of origin software. The strong interaction corresponds to 3343 cm^{-1} is the hydroxl group which is due to the transmittance rate. The Hirshfield analysis provides intermolecular interactions in the crystal structure. It explains the stabilization i.e. if the bond is strong or weak. The red area and blue area are identified. The red area represents the acceptor level and the blue corresponds to the donor level. The fingerprint plot highlights the inter and intramolecular interactions; acceptor-donor levels are understood. The polarizability and hyperpolarizability of the compound with their static and frequency-dependent characters have been studied and compared with other similar compounds.

6.2. FUTURE SCOPE

Quantum chemical calculation (DFT) study gives a wide area in the molecular world. We can predict different kinds of properties before experimentally done. Our compound shows high charge transfer interaction between central ligand transfer. So it may be used for the application of NLO studies such as switching properties in the optical limiters etc.

REFERENCES

1. Philos Trans A Math Phys Eng Sci. 2014 Mar 13; 372(2011): 20120488.

2. Kohn, Walter, Axel D. Becke, and Robert G. Pagencrr. "Density functional theory of electronic structure." The journal of physical chemistry 100.31 (1996): 12974-12980

3. Zhang, Ying, et al. "Mechanistic understanding of the electrocatalytic CO2 reduction reaction–New developments based on advanced instrumental techniques." *Nano Today* 31 (2020): 100835.

4. Philos Trans A Math Phys Eng Sci. 2014 Mar 13; 372(2011): 20120488. doi: 10.1098/rsta.2012.0488

5. Liebman, Joel F. "Book Review: Density Functional Theory: A Practical Introduction, by David S. Sholl and Janice A. Steckel, John Wiley & Sons, 2009; xii+ 238 pages; $90.00; ISBN 978-0-470-37317-0." (2009): 249-250.

6.Liebman, J. F. (2009). Book Review: Density Functional Theory: A Practical Introduction, by David S. Sholl and Janice A. Steckel, John Wiley & Sons, 2009; xii+ 238 pages; $90.00; ISBN 978-0-470-37317-0.

7. Zielinski, Theresa Julia, et al. "Quantum states of atoms and molecules." (2005): 1880

8.Sholl, David S., and Janice A. Steckel. Density functional theory: a practical introduction . John Wiley&Sons,2022.

9.A. J . Cohen and N.C.Handy,J.Chem.Phys.117,1470(2002)

10. Hill, J. Grant. "Gaussian basis sets for molecular applications." International Journal of Quantum Chemistry 113.1 (2013): 21-34.

11.Vande Vondele, Joost, and Jürg Hutter. "Gaussian basis sets for accurate calculations on molecular systems in gas and condensed phases." The Journal of Chemical Physics 127.11 (2007).

12. Slater, John C. "A simplification of the Hartree-Fock method." Physical review 81.3 (1951): 385.

13. Boyd, R. (2012). *Contemporary nonlinear optics*. Academic Press.

14. Aruldhas, G. Quantum mechanics. PHI Learning Pvt. Ltd., 2008.

15.Boyd, Robert W., Alexander L. Gaeta, and Enno Giese. "Nonlinear optics." Springer Handbook of Atomic, Molecular, and Optical Physics. Cham: Springer International Publishing, 2008. 1097-1110.

16.Laud, B. B. (1986). Lasers and nonlinear optics.

17.Mitrić, Jelena. "Properties and characterization of rare-earth-activated phosphors." *Rare-Earth-activated Phosphors*. Elsevier, 2022. 69-84.

18.Weinhold, F., C. R. Landis, and E. D. Glendening. "What is NBO analysis and how is it useful?." *International reviews in physical chemistry* 35.3 (2016): 399-440.

APA

19. Moolya, B. Narayana, et al. "Hydrogen bonded nonlinear optical γ-glycine: crystal growth and characterization." *Journal of Crystal Growth* 280.3-4 (2005): 581-586.

20.Reed, Alan E., Larry A. Curtiss, and Frank Weinhold. "Intermolecular interactions from a natural bond orbital, donor-acceptor viewpoint." Chemical Reviews 88.6 (1988): 899-926.

21. Zhao, Tongpeng, et al. "Structural design and characterization of a chalcone derivative crystal DAMO with strong SHG efficiency for NLO applications." *Optical Materials* 112 (2021): 110765.

22.Boukabene, Mohamed, et al. "Theoretical study of geometric, optical, nonlinear optical, UV–Vis spectra and phosphorescence properties of iridium (III) complexes based on 5-nitro-2-(2′, 4′-difluorophenyl) pyridyl." *Theoretical Chemistry Accounts* 139.3 (2020): 47.

23.Steve Scheiner, in Intra- and Intermolecular Interactions Between Non-covalently Bonded Species, 2021

24.https://www.google.com/url?sa=i&url=https%3A%2F%2Fwww.nlosource.com%2FPolarizability.html&psig=AOvVaw2d4WypPYsxloP20GxCmxPb&ust=1713931506760000&source=images&cd=vfe&opi=89978449&ved=0CAcQrpoMahcKEwjQ-c3IuteFAxUAAAAAHQAAAAAQBA

25. Kamal, Samrah, et al. "Synthesis, characterization and DFT studies of water stable Cd (II) metal–organic clusters with better adsorption property towards the organic pollutant in waste water." *Inorganica Chimica Acta* 512 (2020): 119872.

26.https://www.google.com/url?sa=i&url=https%3A%2F%2Fjncollegeonline.co.in%2Fattendence%2Fclassnotes%2Ffiles%2F1627142910.pdf&psig=AOvVaw3oLB_XG7Vgjalxu-eE-Qif&ust=1713942461450000&source=images&cd=vfe&opi=89978449&ved=0CAcQrpoMahcKEwiA1NKv49eFAxUAAAAAHQAAAAAQBA

27.Buckingham, Amyand David. "Polarizability and hyperpolarizability." *Philosophical Transactions of the Royal Society of London. Series A, Mathematical and Physical Sciences* 293.1402 (1979): 239-248.

28. Liyanage, Poornima S., Rohini M. de Silva, and KM Nalin de Silva. "Nonlinear optical (NLO) properties of novel organometallic complexes: high accuracy density functional theory (DFT) calculations." *Journal of Molecular Structure: THEOCHEM* 639.1-3 (2003): 195-201.

29.Mostaço-Guidolin, Leila, Nicole L. Rosin, and Tillie-Louise Hackett. "Imaging collagen in scar tissue: developments in second harmonic generation microscopy for biomedical applications." *International journal of molecular sciences* 18.8 (2017): 1772.

30. Mendes, Paulo J., AJ Palace Carvalho, and JP Prates Ramalho. "Role played by the organometallic fragment on the first hyperpolarizability of iron–acetylide complexes: A TD-DFT study." *Journal of Molecular Structure: THEOCHEM* 900.1-3 (2009): 110-117.

31.Pongpiacha, Siwatt. "FTIR spectra of organic functional group compositions in PM2. 5 collected at Chiang-Mai City, Thailand during the haze episode in March 2012." *Journal of Applied Sciences* 14.22 (2014): 2967-2977.

32.FTIR SPECTROSCOPIC STUDIES ON CLEOME GYNANDRA – COMPARATIVE ANALYSIS OF FUNCTIONAL GROUP BEFORE AND AFTER EXTRACTION - Scientific Figure on ResearchGate. Available from: https://www.researchgate.net/figure/FTIR-frequency-range-and-functional-groups-present-in-the-sample-after-extraction-process_tbl3_255486350 [accessed 18 Apr, 2024]

33.https://www.sciencedirect.com/topics/chemistry/hyperpolarizability#:~:text=Lucjan%20Piela%2C%20in,%2C%202020

34.Bonin, Keith D., and Vitaly V. Kresin. *Electric-dipole polarizabilities of atoms, molecules, and clusters*. World Scientific, 1997.

35. NIKOLAI V. TKACHENKO, in Optical Spectroscopy, 2006

36.I. Biaggio, in Handbook of Organic Materials for Optical and (Opto)electronic Devices, 2013

37.Dziedzic, J. M., Roger H. Stolen, and Arthur Ashkin. "Optical Kerr effect in long fibers." *Applied optics* 20.8 (1981): 1403-1406.

38.https://www.mdpi.com/chemproc/chemproc-14-00092/article_deploy/html/images/chemproc-14-00092-g002.png

39. Bojarska, Joanna, et al. "The experimental and theoretical landscape of a new antiplatelet drug ticagrelor: Insight into supramolecular architecture directed by CH··· F, π··· π and CH··· π interactions." *Journal of Molecular Structure* 1154 (2018): 290-300.

40. Spackman, Mark A., and Dylan Jayatilaka. "Hirshfeld surface analysis." *CrystEngComm* 11.1 (2009): 19-32.

41.Champagne, Benoît. "Polarizabilities and hyperpolarizabilities." (2009).

Figures

[1] **https://doi.org/10.1002/wcms.34**

[2] https://www.tribonet.org/wp-content/uploads/2022/10/word-image-63804-1.png.webp

[3]: https://ieeexplore.ieee.org/stamp/stamp.jsp?tp=&arnumber=6270425&isnumber=6270417

[4] https://www.researchgate.net/profile/Viet-Nguyen-Ai/publication/274265027/figure/fig2/AS:316976296677377@1452584446420/Energy-diagram-of-two-state-quantum-system.png